IJHSR
ijhighschoolresearch.org
RESEARCH ARTICLE

Three-Dimensional Hierarchical Porous Electrode Structure for Improved Performance in Battery Applications

Alan Wang
Westlake High School, 4100 Westbank Dr, Austin, TX 78746, Austin, TX, 78746, USA; alanwang285@gmail.com

ABSTRACT: The demand for lithium-ion batteries is rapidly increasing due to urgent needs for effective renewable energy storage. Particularly, attention has shifted towards thick electrodes, as they optimize the amount of active material in multi-battery systems, increasing the energy densities of these systems; however, thick electrodes lose capacity and stability at high output rates due to their low porosity. Current research aims to solve this by utilizing nanotechnology to create porous structures in cathode materials that greatly increase ion transport rates. Cathode materials are primarily studied since they reach 20% of anode capabilities, limiting overall performance. Previous studies have created porous channels and nanopore structures within cathode materials, but these approaches fail to resolve the inert problems of thick electrodes. This project presents a uniform three-dimensional porous network in $LiCoO_2$, a commercialized Lithium-ion battery cathode, using the polymer poly(methyl methacrylate) (PMMA) in both micrometer and nanometer scales as a template. After mixing $LiCoO_2$ with PMMA, the mixture is heated at high temperatures to burn out PMMA and sinter the templated $LiCoO_2$ powder into a monolithic electrode. The micrometer-sized pores enhance ion conductivity by shortening ion diffusion pathways, and the nanometer-sized pores improve stability by evenly distributing the battery electrolyte. Compared with commercial standards, these electrodes had up 200% greater specific capacities and 51.1% better capacity retention at high output rates, results that can be applied to numerous battery applications. This study furthers 3D nanostructure understanding and opens discussion about dual-scale porosity.

KEYWORDS: Materials Science; Nanomaterials; Energy Storage; Thick Electrodes; Porosity.

Introduction

Battery-powered devices and systems are becoming increasingly prevalent in the 21st century, as they are clean forms of energy. One of the most promising types of batteries are lithium-ion (Li-ion) batteries due to their higher energy and power densities (energy density: total amount of energy stored divided by the mass of battery; power density: rate at which electricity can be charged/discharged divided by the mass of battery), longer cycle life, and greater efficiency compared to other rechargeable battery types such as lead acid, nickel cadmium, sodium sulfur, and sodium nickel chloride.[1] Some of the popular applications for Li-ion batteries include electric vehicles, mobile devices, and robotic systems.[2] Li-ion batteries are also applicable in conjunction with energy-harvesting systems such as solar, wind and hydroelectric forms of energy.[3] While Li-ion batteries have become substantially better recently with greater energy densities, better cycling stability, faster charge/discharge rates, and lower costs, their electrochemical performance is still not sufficient to store enough energy from renewable sources to completely replace fossil fuels. Currently, cathode materials are the limiting factor in Li-ion battery cells for energy density. Anode materials such as graphene and magnetite (Fe_3O_4) can reach specific capacities of 400-1000 mAh g-1, while cathode materials such as $LiCoO_2$ and $LiFePO_4$ can only reach specific capacities of 140-170 mAh g-1.[4,5] Thus, to create Li-ion electrodes with greater energy densities and faster rate capabilities, areal mass of cathodes must be improved to meet anode capabilities.

With the introduction of nanotechnology in the past few decades, efforts to improve Li-ion battery performance are now focused on modifying the morphology (dimensions, weight, volume, porosity, structure) of existing materials. There are several methods to improve electrode energy density in Li-ion batteries, such as templating composite structures, doping cathode structures with other metals, carbon coating electrode material, and modifying electrolyte composition.[6,7] However, current efforts are mainly directed towards modifying electrode structure on a nanoscale to increase electrode porosity, especially in thick electrodes as they provide greater energy density in battery applications due to a greater ratio of active to inactive material.[8,9] Before this study, several other studies have created porous, thick cathodes using various methods such as utilizing wood's microscopic structure as a template, implementing magnetic alignment, and using laser processing to produce aligned porous channels within the cathode.[10-12] When cathode particles are oriented in channels, porosity is controlled, which increases the energy density, cycling stability, electronic conductivity in electrodes. Nevertheless, the overall density of the electrode remains relatively similar to an unmodified electrode since the pore channels are merely embedded into the electrode as better pathways for ion diffusion, but electrode areas without grooves still have the same properties as an unmodified thick electrode. Hence, while electrodes with porous channels may initially have high specific capacities and rate performance, they rapidly lose capacity at higher output rates. Additionally, metal oxides with mesoporous structures have also resulted in greater electrochemical properties such as greater energy and power densities due to a uniform and continuous pore network that permits efficient transport of electrons and ions while

DOI: 10.36838/v4i5.1

allowing fluids to pass through the internal structure.[13,14] Thus, when an electrolyte is applied to the mesoporous cathode structure, the interconnected pores cause a uniform distribution of the electrolyte, which decreases short circuit possibilities and produces more stable electrodes. While both processes modify thick electrode structure by controlling porosity, spherical polymer templating in a hierarchical format has not been utilized to create a uniformly porous electrode in combination with macropores. Moreover, several papers have adopted a hierarchical porosity strategy to improve electrode performance.[15-17] Bae *et al.* also studied $LiCoO_2$, however they implemented dual-scale pore channels into their electrode. Kwon *et al.* synthesized 3D pores by reacting GeO_2 with Zn to form pores within the Ge anode material. Vu *et al.* implemented a Carbon composite within a $LiFePO_4$ electrode to create a dual-scale porosity with nanopores. However, this study is different from these previous works as they have not introduced hierarchical porosity in both a micrometer and nanometer scale using polymer templating.

Through nanotechnology, electrode morphology and porosity can be modified at the nanoscale to increase battery performance. In this project, the porosity in $LiCoO_2$ (LCO) electrodes is controlled by creating a hierarchical pore network in a monolithic (monolith: single piece of material) thick-electrode (>300 µm thickness) using the spherical polymer poly(methyl methacrylate) (PMMA) in both a nano-size (~300 nm in diameter) and a micrometer size (30-80 µm in diameter) as templates. Both pore sizes increase ion transport rates and the surface area of the electrode. However, with the combination of the nano-sized pores and micro-sized pores, an interconnected porous network allows uniform electrolyte diffusion throughout the electrode. It is hypothesized that constructing ultra-thick free-standing monolith electrodes with a three-dimensional (3D) hierarchically interconnected pore network in Li-ion batteries will improve ion transport kinetics along the diffusion direction. Consequently, commercial LCO composite electrodes will have higher material utilization with an increased energy density while maintaining high power density, leading to more effective usage of renewable energy. Figure 1 captures the potential applications of a 3D hierarchically porous, thick LCO cathode (3D LCO) through a schematic illustration of the synthesis principle and outcome as well as the assembly process for experimentation battery cells. The experimentation battery cells used in this project were half coin cells (C-2032; Half Coin Cell: Li-ion battery assembled with only cathode material and lithium metal as anode to restrict results to cathode capabilities), and each cell contains a positive case, current collector, 3D LCO cathode monolith, liquid battery electrolyte, Li-metal, metal spacer, metal spring, and negative case. The liquid battery electrolyte is depicted on both sides of the separator since even though it is applied on top of the separator, the electrolyte imbues throughout the separator material, which coats both the cathode and the Li-metal.

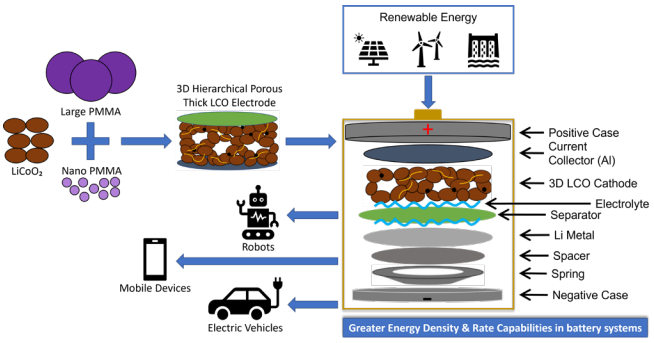

Figure 1: Schematic illustration of various applications of 3D hierarchical porous, thick LCO electrode with C-2032 coin cell assembly.

Methods

This section summarizes the procedures required to synthesize and test Li-ion battery cells using 3D LCO as a cathode in a Li-ion half-cell. Figure 2 depicts a flow chart of the experimental procedures with the utilized research equipment and the specified products at each step of the experimental process.

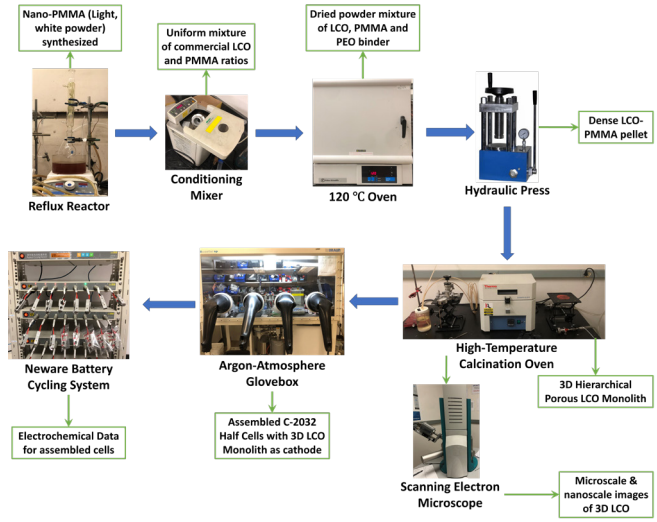

Figure 2: Schematic flow chart of experimental procedures required to synthesize, assemble, and test half Li-ion cells with 3D LCO monoliths as the cathode material (blue arrows: experimental steps; green arrows/boxes: attained products at specified steps).

Nanometer-sized PMMA Synthesis:

Nanometer-sized PMMA (nano PMMA) was synthesized via emulsion polymerization of the monomer methyl methacrylate (MMA), according to Peng *et al.*[18] First, 0.002 g sodium dodecyl sulfate was dissolved in 50 mL deionized water as a surfactant (surfactant: chemical agent that decreases solvent surface tension to permit effective reaction between different substances). Next, 7 g methyl methacrylate monomer and 0.056 g potassium peroxodisulfate, the initiator (initiator: chemical agent that initiates the polymerization process), were dissolved into the solution with continuous magnetic stirring. After, the solution underwent a reflux system reaction bubbled with nitrogen gas for 20 minutes to ensure that all oxygen gas was removed. Then, the reflux system was stirred for 2.5 hours at 70 °C to ensure reaction completion. After, the remaining solution was centrifuged and inserted into a 120 °C oven to dry so all solvents were evaporated.

3D Hierarchical Porous $LiCoO_2$ Monolith Synthesis:

Various PMMA ratios were tested to find the best performing measurements, but all monolith samples had 250 mg of $LiCoO_2$ active commercial powder (Sigma Aldrich), 50 mg PMMA (large and/or small), and 0.025 mL 10% weight polyethylene oxide (PEO)-lithium bistriflimide (TFSI) in acetonitrile solution (PEO solution serves as polymer binder between $LiCoO_2$ and PMMA). The PMMA ratios tested were 25 mg small PMMA with 25 mg large PMMA (25s/25L), 40 mg small PMMA with 10 mg large PMMA (40s/10L), and 50 mg small PMMA (50s). $LiCoO_2$ and respective PMMA amounts were first mixed using a conditioning mixer (Thinky Mixer AR-100) for 30 minutes to create a uniform mixture of $LiCoO_2$ and PMMA. Then, the LCO:PMMA mixture was ground together with the PEO-TFSI solution in a mortar and pestle for about 2 minutes until the mixture was powdered. After, 100 mg samples were weighed out and diced on a glass board to ensure material particle size uniformity, then dried for about 5 minutes in a 120 °C oven so the PEO-TFSI solvent was evaporated. Then, each sample was inserted into a hydraulic press for 1 minute at a pressure of 10 tons to create 3D hierarchically porous LCO (3D LCO) pellets. Afterward, each pellet was placed on a bed of commercial $LiCoO_2$ and calcined from 20 °C to 400 °C at a 2 °C /min ramping rate, then held at 400 °C for 2 hours, then heated 400 °C to 850 °C at a rate of 1 °C/min, then held at 850 °C for 2 hours, then cooled to room temperature naturally. The 3D LCO pellets were then placed on a bed of commercial LCO so that surface pore sites on the pellet would also be covered by LCO. The calcination oven was first set to a temperature of 400 °C to burn out the PMMA templates and PEO binder and was then set to 850 °C to sinter the electrode to form a single solid monolith material from the initial powder sample.

Electrode Assembly:

Once 3D LCO monolith has successfully been calcinated, the final step was electrode assembly. First, 10% conductive carbon (Super P) in N-methylpyrrolidone (NMP) solution was drop-casted onto the monolith until the monolith was sufficiently coated so that the monolith's surface and pores would both be covered by conductive carbon. Next, the monoliths were inserted into a vacuum oven at 120 °C overnight to evaporate the NMP solvent. After the monoliths were dry, 2032 half coin battery cells were assembled with the current collector, the monolith as the electrode, a separator, about 0.1 mL 1.0 M $LiPF_6$ (dissolved in 50/50 mixture of Ethylene Carbonate and Diethyl Carbonate) electrolyte solution Li-metal plate, a metal spacer, and a metal spring and tested on a Neware cycling machine system.

Results and Discussion

This section presents the results gathered for the 25s/25L, 40s/10L, and 50s samples after synthesis. Micrometer and nanometer scale images were taken by a Scanning Electron Microscope (SEM, Vega3 Tescan & Quanta FEG) and electrochemical data was tracked by a Neware battery testing system (Neware BT4000) for half coin cells containing 3D LCO.

Morphology Analysis :

In Figure 3, a schematic illustration for the electrode design of the 3D LCO electrode is shown. Figures 3a and 3b represent current thick electrodes, and Figures 3c, 3d, 3e, and 3f represent the newly synthesized 3D porous LCO electrode.

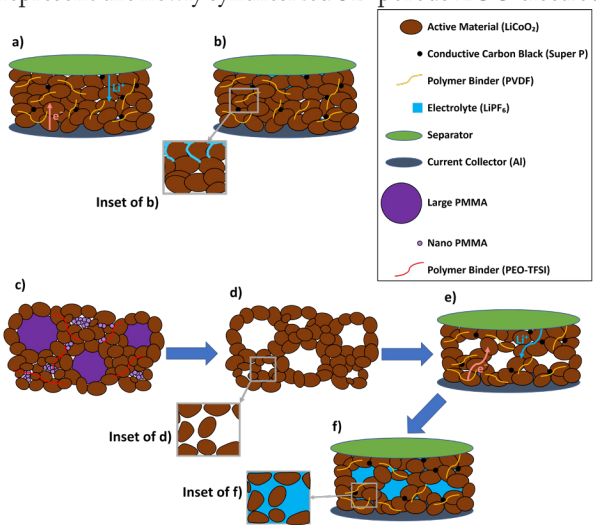

Figure 3: a: Thick LCO commercial electrode (Control); b: Control electrode with electrolyte; inset of b: Nanoscale depiction of electrolyte diffusion in control electrode; c: LCO mixed with large and nano PMMA before sintering; d: 3D porous LCO electrode after sintering; inset of d: Nanoscale depiction of 3D LCO electrode after sintering; e: 3D LCO electrode with conductive carbon and polymer binder; f: 3D LCO electrode with electrolyte; inset of f: Nanoscale depiction of electrolyte diffusion in 3D LCO.

As seen in Figures 3a and 3b, current thick electrodes cause Li ions to have much longer ion transport rates due to their lack of porosity and higher density. This causes thick electrodes to have worse rate performance than thin electrodes. In inset of Figure 3b, electrolyte diffusion is shown at the nanoscale. Due to the lack of porosity, the electrolyte remains near the top of the application spot, causing an uneven electrolyte distribution, which leads to significantly worse ion transport kinetics. Figure 3c depicts the initial mixing between LCO, large PMMA, nano PMMA, and the PEO-TFSI polymer binder. After sintering the electrode at high temperatures, Figure 3d shows the monolith product. Figure 3d's inset displays the electrode on a nanoscale and how mesopores formed by nano PMMA aggregates are present. Figure 3e displays the Li ion and electron pathways in the 3D LCO electrode, which have faster rates due to the increased porosity. Figure 3f shows electrolyte diffusion in the 3D LCO electrode, and the inset of Figure 3f illustrates how by adding nano PMMA into the electrode, the electrolyte can evenly spread throughout the electrode, allowing for greater ion transport kinetics.

To verify the existence of both large and small pores, SEM was used to observe the morphology, uniformity, and material size. In Figure 4, SEM images of large PMMA and nano-PMMA are shown respectively in 4a and 4b. Figures 4c, 4d, and 4e are images of the 25S/25L, 40S/10L, and 50S 3D LCO samples respectively at a 50 μm scale. In Figures 4f, 4g, and 4h, images of 25S/25L, 40S/10L, and 50S LCO samples

DOI: 10.36838/v4i5.1

are shown respectively at a 200 µm scale. The large PMMA in Figure 4a is shown to have a diameter of 30-80 µm, while nano PMMA particles have a diameter of ~300 nm. However, Figure 4b portrays how nano PMMA particles tend to aggregate, which causes the micropores found in Figures 4e and 4h. Figures 4c and 4d have clear evidence of larger micropores, whereas Figure 4e solely contains smaller micropores formed from nano PMMA. As seen in Figures 4f, 4g, and 4h, the samples had uniform LCO distribution throughout the material. Additionally, as the amount of nano PMMA added to each sample increased, the density of the material decreased due to a greater presence of micropores, shown in comparison between Figures 4f and 4h.

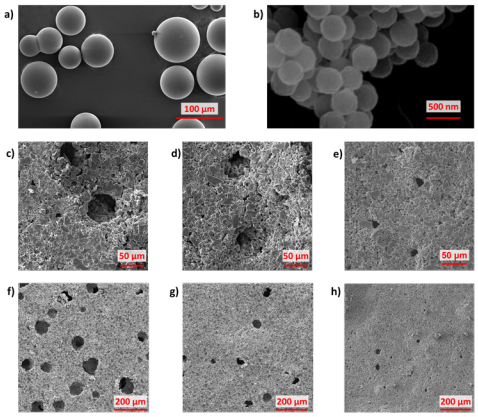

Figure 4: a: Large PMMA at 100 µm scale; b: Nano PMMA at 500 nm scale; c: 25S/25L LCO at 50 µm scale; d: 40S/10L LCO at 50 µm scale; e: 50S LCO at 50 µm scale f: 25S/25L LCO at 200 µm scale; g: 40S/10L LCO at 200 µm scale; h: 50S LCO at 200 µm scale

To determine the pore size distribution, histograms tracking pore diameter percentages for the 25S/25L, 40S/10L, and 50S samples (Figures 5a, 5b, and 5c respectively) at the 200 µm scale were created. Each histogram was created using an average of eight photos taken at various sites of the electrode, and pore diameter was found using ImageJ line drawing. In the 25S/25L and 40S/10L samples, most pores were in the projected 30-80 µm range, but there were some pores in the 80-90 µm range. These outliers are likely due to two large PMMA particles aggregating together, like the PMMA particles in the upper left corner of Figure 4a. In the 50S sample, aggregated nano PMMA particles mainly formed pores of 10-20 µm in diameter but some larger aggregates formed pores of 20-40 µm in diameter.

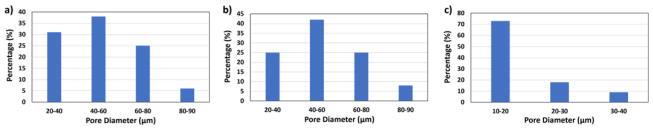

Figure 5: a: 25S/25L averaged pore histogram at 200 µm scale; 40S/10L averaged pore histogram at 200 µm scale; 50S averaged pore histogram at 200 µm scale

Electrochemical Data:

Specific Capacity (mAh g^{-1}) vs. Voltage (V), C-Rate vs. Specific Capacity (mAh g^{-1}), and C-Rate vs. Capacity Retention (%) plots for the 25S/25L, 40S/10L, and 50S LCO samples are shown in Figures 6a, 6b, and 6c respectively. These plots also include data from a standard thick electrode (~270 µm thick) to compare results with commercial capabilities. All values used for Figure 6 correspond with the discharge performance of the four cell types. From the plots in Figure 6a, all four cells reached a mid-voltage of ~3.9V at a rate of 0.1C. Additionally, all four cells had stable discharge output at a 0.1C rate as specific capacity increased, which is shown by the relatively flat middle section of the plots. However, at a 1C rate, as voltage declined, disparities between maximum specific capacities became evident. While the commercial electrode fell to a maximum capacity of 20 mAh g-1, the 25S/25L and 50S electrodes reached capacities of ~40 mAh g-1, and the 40S/10L electrode even reached a capacity of ~60 mAh g-1. As shown in Figure 6b, a large gap in specific capacity between the commercial electrode and the three 3D LCO samples forms at 0.3C that persists until 1C, revealing a significant difference in stability at higher output rates. In addition, although both the 3D LCO samples and commercial electrode decreased in capacity, the decrease rate for the commercial electrode was far greater than the rate for the 3D LCO electrodes, particularly between 0.2C to 0.5C. From Figure 6c, the capacity retention in the 25S/25L, 40S/10L, and 50S samples performed at similar efficiencies from 0.1C-1C, while the commercial electrode fell rapidly from 0.2C-0.5C. At 0.5C, the highest difference in capacity retention, at 51.1%, was between the 40S/10L and commercial electrode.

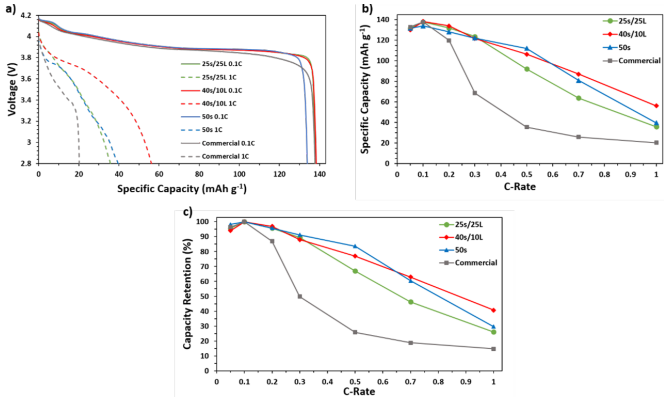

Figure 6: a: Specific Capacity (mAh g−1) vs. Voltage (V) plots of 3D LCO and commercial electrodes at 0.1C and 1C; b: Cycle Number vs. Specific Capacity (mAh g−1) plots of 3D LCO and commercial electrodes; c: Cycle Number vs. Capacity Retention (%) of 3D LCO and commercial electrodes

■ Conclusions & Future Work

In this study, $LiCoO_2$ thick electrodes with three-dimensional hierarchical pores were fabricated through polymer templating using poly(methyl methacrylate) in both micrometer and nanometer sizes. By creating an LCO electrode with a uniform pore distribution of both nanometer and micrometer pores, both electrode energy density and electrode stability are improved at all C-Rates.

The three tested samples all outperformed industry standards in energy densities and cell stability. The best performing sample, the 40S/10L ratio, had up to 200% greater specific capacities and 51.1% greater capacity retention than commercial standards. These results could potentially add 200 miles/charge to a Tesla Model S and 3 hours of battery life to an iPhone.

DOI: 10.36838/v4i4.1

conductive carbon to be more uniformly integrated in the material.

Additional future studies could include testing this synthesis approach with different cathode and anode materials, determining why trends in pore size distribution form, tracking Coulombic efficiency for these samples, and optimizing the nano and micro PMMA ratio.

Acknowledgements

The author greatly appreciates the support of this research from the Walker Department of Mechanical Engineering at the University of Texas at Austin, and particularly acknowledges Professor Guihua Yu and Dr. Xiao Zhang for their extensive help in scanning electron microscopy imaging, coin cell assembly, and research guidance.

References

1. Guney, M. S., & Tepe, Y. (2017). Classification and assessment of Energy Storage Systems. Renewable and Sustainable Energy Re views, 75, 1187–1197. https://doi.org/10.1016/j.rser.2016.11.102.. https://pubmed.ncbi.nlm.nih.gov/31467682/
2. Yang, Y., Okonkwo, E. G., Huang, G., Xu, S., Sun, W., & He, Y. (2021). On the sustainability of lithium ion battery industry – a review and perspective. Energy Storage Materials, 36, 186–212. https://doi.org/10.1016/j.ensm.2020.12.019.
3. Diouf, B., & Pode, R. (2015). Potential of lithium-ion batteries in renewable energy. Renewable Energy, 76, 375–380. https://doi.org/10.1016/j.renene.2014.11.058.
4. Goriparti, S., Miele, E., De Angelis, F., Di Fabrizio, E., Proietti Zaccaria, R., & Capiglia, C. (2014). Review on recent progress of nanostructured anode materials for Li-ion batteries. Journal of Power Sources, 257, 421–443. https://doi.org/10.1016/j.jpowsour.2013.11.103.
5. Fergus, J. W. (2010). Recent developments in cathode materials for lithium ion batteries. Journal of Power Sources, 195(4), 939–954. https://doi.org/10.1016/j.jpowsour.2009.08.089.
6. Zhang, X., Hui, Z., King, S., Wang, L., Ju, Z., Wu, J., Takeuchi, K. J., Marschilok, A. C., West, A. C., Takeuchi, E. S., & Yu, G. (2021). Tunable porous electrode architectures for enhanced Li-ion storage kinetics in thick electrodes. Nano Letters, 21(13), 5896–5904. https://doi.org/10.1021/acs.nanolett.1c02142.
7. Jyoti, J., Singh, B. P., & Tripathi, S. K. (2021). Recent advancements in development of different cathode materials for rechargeable lith ium ion batteries. Journal of Energy Storage, 43, 103112. https://doi.org/10.1016/j.est.2021.103112.
8. Singh, M., Kaiser, J., & Hahn, H. (2015). Thick electrodes for high energy lithium ion batteries. Journal of The Electrochemical Soci ety, 162(7). https://doi.org/10.1149/2.0401507jes.
9. Wu, J., Zhang, X., Ju, Z., Wang, L., Hui, Z., Mayilvahanan, K., Takeuchi, K. J., Marschilok, A. C., West, A. C., Takeuchi, E. S., & Yu, G. (2021). From fundamental understanding to engineering design of high-performance thick electrodes for scalable energy-storage systems. Advanced Materials, 33(26), 2101275. https://doi.org/10.1002/adma.202101275.
10. Lu, L.-L., Lu, Y.-Y., Xiao, Z.-J., Zhang, T.-W., Zhou, F., Ma, T., Ni, Y., Yao, H.-B., Yu, S.-H., & Cui, Y. (2018). Wood-in spired high-performance ultrathick bulk battery electrodes. Ad vanced Materials, 30(20), 1706745. https://doi.org/10.1002/adma.201706745.
11. Sander, J. S., Erb, R. M., Li, L., Gurijala, A., & Chiang, Y.-M. (2016). High-performance battery electrodes via magnetic templating. Nature Energy, 1(8). https://doi.org/10.1038/nener gy.2016.99.
12. Park, J., Jeon, C., Kim, W., Bong, S.-J., Jeong, S., & Kim, H.-J. (2021). Challenges, laser processing and electrochemi cal characteristics on application of ultra-thick electrode for high-energy lithium-ion battery. Journal of Power Sources, 482, 228948. https://doi.org/10.1016/j.jpowsour.2020.228948.
13. Peng, L., Fang, Z., Zhu, Y., Yan, C., & Yu, G. (2017). Holey 2d nanomaterials for electrochemical energy storage. Advanced Energy Materials, 8(9), 1702179. https://doi.org/10.1002/aenm.201702179.
14. Celik, E., Ma, Y., Brezesinski, T., & Elm, M. T. (2021). Ordered mesoporous metal oxides for electrochemical applications: Cor relation between structure, electrical properties and device per formance. Physical Chemistry Chemical Physics, 23(18), 10706–10735. https://doi.org/10.1039/d1cp00834j.
15. Bae, C.-J., Erdonmez, C. K., Halloran, J. W., & Chiang, Y.-M. (2012). Design of battery electrodes with dual-scale porosity to minimize tortuosity and maximize performance. Advanced Materials, 25(9), 1254–1258. https://doi.org/10.1002/adma.201204055.
16. Kwon, D., Ryu, J., Shin, M., Song, G., Hong, D., Kim, K. S., & Park, S. (2018). Synthesis of dual porous structured germanium an odes with exceptional lithium-ion storage performance. Journal of Power Sources, 374, 217–224. https://doi.org/10.1016/j.jpowsour.2017.11.044.
17. Vu, A., & Stein, A. (2011). Multiconstituent synthesis of LiFePO4/C composites with hierarchical porosity as cathode ma terials for lithium ion batteries. Chemistry of Materials, 23(13), 3237–3245. https://doi.org/10.1021/cm201197j.
18. Peng, J., Zhang, T., Zhang, H., Zhang, Z., Li, Z., Lei, G. (2012). Synthesis and electrochemical performance of three-dimen sionally ordered macroporous licoo2. Journal of Solid State Elec trochemistry, 16(9), 3079–3085. https://doi.org/10.1007/s10008-012-1752-1.

Author

Alan Wang is a junior at Westlake High School in Austin, Texas. He is interested in studying energy systems and the intersection between materials science and electrical engineering in the future.

DOI: 10.36838/v4i5.1